September 1987 LIDS-P-1710

OBJECT SHAPE ESTIMATION FROM TOMOGRAPHIC MEASUREMENTS — A PERFORMANCE ANALYSIS[1]

David J. Rossi[2]

Alan S. Willsky[3]

Abstract

The problem is considered of determining the shape of an object embedded within a medium from noisy tomographic projection measurements. In particular, the issue is addressed of how accurately coarse features of object geometry -- size, elongation and orientation -- can be characterized from noisy projection data. A Maximum Likelihood parameter estimation formulation is used and estimation performance is analyzed by evaluation of the Cramer-Rao lower bound on the error variances of the estimates. It is demonstrated that for measurements available at all projection angles and at a given noise level (1) object size and orientation are more accurately determined than is the degree of object elongation, and (2) reliable orientation estimation requires a minimum degree of object elongation, and the required degree of elongation is inversely related to the measurement signal-to-noise ratio (SNR).

---

[1]This work was supported in part by the National Science Foundation under Grant ECS-8700903 and in part by the Army Research Office under Grant DAAL03-86-K-0171.

[2]E.P. Schlumberger, 26 rue de la Cavee, Clamart, France.

[3]Department of Electrical Engineering and Computer Science, and Laboratory for Information and Decision Systems, M.I.T., Room 35-437, Cambridge, MA 02139.

OBJECT SHAPE ESTIMATION FROM TOMOGRAPHIC MEASUREMENTS – A PERFORMANCE ANALYSIS

David J. Rossi[1]

Alan S. Willsky[2]

ABSTRACT

The problem is considered of determining the shape of an object embedded within a medium from noisy tomographic projection measurements. In particular, the issue is addressed of how accurately coarse features of object geometry – size, elongation and orientation – can be characterized from noisy projection data. A Maximum Likelihood parameter estimation formulation is used and estimation performance is analyzed by evaluation of the Cramer-Rao lower bound on the error variances of the estimates. It is demonstrated that for measurements available at all projection angles and at a given noise level (1) object size and orientation are more accurately determined than is the degree of object elongation, and (2) reliable orientation estimation requires a minimum degree of object elongation, and the required degree of elongation is inversely related to the measurement signal-to-noise ratio (SNR).

I. INTRODUCTION

The problem of reconstructing a multi-dimensional function from its projections arises in a diversity of disciplines, typically in imaging applications. In these applications, one is interested in determining a profile characterizing the interior of a medium (e.g., x-ray attenuation coefficient) from integral or projection-type measurements obtained by external probing of the medium.

One popular application is medical x-ray CAT scanning, where x-rays are directed along a collection of straight lines lying in a plane intersecting the patient; the set of projection measurements so obtained are used to reconstruct the x-ray attenuation profile within the cross-section. Recently, a number of novel applications of similar reconstruction techniques has been explored, for example mesoscale oceanographic thermal mapping, quality control nondestructive evaluation, geophysical tomography and "stop action" imaging of very

rapidly changing media [1-5]. In contrast to medical CAT scanning, many of these applications are characterized by measurement limitations due, for example, to limitations in the number of measurement transducers, constraints on measurement time, or operational constraints limiting measurement view angle and/or SNR. These represent severe restrictions when the goal is to produce high resolution, artifact-free cross-sectional imagery, for it is well known that when the projection measurements are limited or noisy, the reconstruction inverse problem is ill-posed, having a numerically sensitive or noisy solution [6].

In a number of applications, particularly with limited measurement data, the *ultimate* goal of the processing is far more modest than obtaining high resolution cross-sectional imagery. More typically the objective involves quantitative and/or qualitative assessment of objects, regions or boundaries within the cross-section, e.g., thermal regions in ocean mapping, cracks and flaws in nondestructive material evaluation and certain anatomical features in medical scanning [7,8]. The focus of this paper is on the processing of limited or noisy tomographic projection data when the goals involve characterizing *objects* or *regions* in the medium. We model the unknown medium as the superposition of a background medium and one or more local variations in the medium corresponding to objects. Further, each object is characterized by a small set of parameters corresponding, for example, to object location, size, and boundary shape. This type of representation has previously been used to analyze the problem of locating an object from tomographic measurements [9,10], where it was shown that the accuracy of object localization is characterized by a threshold behavior – for a given measurement geometry and measurement noise level, one can identify the smallest size of object that can be reliably located.

In the present paper, that work is extended to the problem of determining, from noisy projection measurements obtained by probing the exterior of a medium, the geometry of an object embedded within the medium. One question to be addressed is how accurately object geometry can be characterized from full-view data (projection measurements acquired from views completely surrounding the object); the limited view angle case may be considered in a similar way. To establish insight, attention is focused in this paper on three attributes characterizing coarse object geometry, specifically size, elongation and orientation. These object attributes are considered as unknown quantities which are estimated directly from

noisy tomographic data using Maximum Likelihood (ML) parameter estimation. The statistical accuracy of these estimates is then characterized by evaluating the Cramer-Rao lower bound (CRLB) on the estimate error variances.

Although the model under consideration is simple, it affords insight into the problem of characterizing object geometry from tomographic data. For example, this analysis may be used to identify, for a given measurement geometry and noise level, the minimum degree of object elongation required to achieve a specified accuracy in object orientation estimation. This analysis also demonstrates that when all three attributes – size, elongation, and orientation – are simultaneously unknown, size and orientation can be estimated substantially more accurately than can the degree of elongation.

The paper is organized as follows. In Section II, notation is reviewed for both the tomographic reconstruction problem and for the object-based profile model described in [9,10]. In Section III the profile model from [9,10] is restricted to objects capturing the three features of object geometry already mentioned – size, elongation and orientation. In Section IV the problem is considered of ML estimation of the object geometry parameters and expressions are obtained for the log likelihood and ambiguity functions which are used to characterize estimation performance. In Section V the problem is specialized to the analytically tractable case of Gaussian objects and estimation accuracy is assessed for the individual problems of estimating size, elongation, and orientation. Conclusions are presented in Section VI. The issue of estimation robustness or sensitivity to modeling errors is not considered in this paper; see [9] for a discussion of these issues.

II. BACKGROUND

We begin by reviewing the reconstruction of a two-dimensional (2D) function from its projections. Let $f(\mathbf{x})$ represent the value of the cross-sectional function (for example, x-ray attenuation coefficient) at a point specified by the vector $\mathbf{x} = (x_1, x_2)'$. The *projection* of $f(\mathbf{x})$ at angle θ is a 1D function $g(t, \theta)$ as shown in Figure 1, which for given values of t and θ is the integral

$$g(t,\theta) = \int_{-\infty}^{\infty} \int_{-\infty}^{\infty} f(\mathbf{x})\delta(t - \mathbf{x}'\Theta)dx_1dx_2 = \int_{\mathbf{x}'\Theta=t} f(\mathbf{x})ds \doteq [\mathbf{R}f](t,\theta) \qquad (1)$$

along the line

$$\ell(t,\theta) = \{\mathbf{x} : x_1 \cos\theta + x_2 \sin\theta = t\} = \{\mathbf{x} : \mathbf{x}'\Theta = t\} \tag{2}$$

$$\Theta \doteq (\cos\theta \quad \sin\theta)' \tag{3}$$

$$(t,\theta) \in S \doteq \{(t,\theta) : -\infty < t < \infty \ , \ 0 \leq \theta < \pi\} \tag{4}$$

as shown in Figure 2. In (1), $\delta(t)$ is the Dirac delta function. The integral equation (1) corresponds to the Radon transformation, which maps the 2D function $f : R^2 \rightarrow R$ into a function on a half-cylinder $g : S \rightarrow R$; $g(t,\theta)$ is called the Radon transform of $f(\mathbf{x})$, and is also denoted by $[\mathbf{R}f](t,\theta)$.

The convolution backprojection (CBP) inversion formula [11] is one solution to the integral equation in (1); it assumes the availability of noise-free measurements at all (t,θ) values on the half-cylinder S, and is given by

$$\hat{f}(\mathbf{x}) = \int_0^{\pi} \int_{-\infty}^{\infty} g(t,\theta) v(t - \mathbf{x}'\Theta, \theta) dt d\theta = \int_0^{\pi} q(\mathbf{x}'\Theta, \theta) d\theta \doteq [\mathbf{B}q](\mathbf{x}) \tag{5}$$

where the convolving kernel $v(t,\theta)$ is θ-independent with a Fourier transform with respect to t satisfying $V(\omega) = \mid \omega \mid$. The so-called *backprojection* operator (the integral with respect to θ) maps the function $q : S \rightarrow R$ into the 2D function $\hat{f} : R^2 \rightarrow R$; $\hat{f}(\mathbf{x})$ is called the backprojection of q and is also denoted by $[\mathbf{B}q](\mathbf{x})$.

In the object-based model from [9,10], the 2D cross-section $f(\mathbf{x})$ is represented as the superposition of a background and N objects,

$$f(\mathbf{x}) = f_b(\mathbf{x}) + \sum_{k=1}^{N} d_k \ f(\mathbf{x} - \mathbf{c}_k; \gamma_k) \tag{6}$$

Here, the k^{th} object is located at the point $\mathbf{c}_k$ and has contrast or density d_k (f is normalized so that $f(0;\gamma_k)$ is unity). The density fluctuations of the k^{th} object are characterized by the finite-dimensional vector of parameters γ_k containing, for example, information about the object boundary shape and interior density fluctuations. The problem of estimating the object location $\mathbf{c}_k$ from noisy projection measurements was considered previously [9,10]. In this paper, the problem of estimating the object geometry parameters γ_k from noisy projection data is considered. For simplicity, and in order to establish insight, it is assumed that the background $f_b(\mathbf{x})$ is known (and without loss of generality taken to equal zero) and

that only a single object (N=1) is present at a known location $\mathbf{c}_1$. The effect of errors in these assumptions is considered in the robustness study in [9], where it is shown that object shape determination is quite robust to errors in the assumed object location and to the presence of additional unmodeled objects having small Radon transform energy (as defined in the next section). The single object in the cross-section is considered to have unknown size, shape and orientation (i.e., γ is unknown) and these parameters are estimated directly from noisy tomographic data. In the following sections, the parameterization of object size, shape and orientation is discussed, and the performance of ML estimation of the geometry parameters is evaluated.

III. REPRESENTATION OF OBJECT SHAPE

There are various ways to characterize the boundary of an object. For example, if the object is convex, its boundary can be parameterized by the coefficients in a series expansion of its support function [7,12]; alternatively, an object boundary may be approximately represented by a sequence of horizontally and vertically directed edge elements [13]. In the present analysis, a parameterization is considered that captures in a simple way three important features of object geometry – size, elongation and orientation. In particular, the object under consideration is approximated as resulting from a simple circularly-symmetric *reference* object by the application of a series of spatial deformations – magnification (size attribute), stretching (elongation attribute) and rotation (orientation attribute).

More specifically, consider a circularly-symmetric *reference* object located at the origin; let it be denoted by $s(\mathbf{x})$, or since it is circularly-symmetric, by $s_p(r)$ in terms of the radial polar coordinate r. The Radon transform of this object is independent of the projection angle θ and is denoted by $g_s(t)$. The energy in the Radon transform is denoted by

$$\xi_s = \int_0^{\pi} \int_{-\infty}^{\infty} g_s^2(t,\theta) dt d\theta \; = \; \pi \int_{-\infty}^{\infty} g_s^2(t) dt \tag{7}$$

The circularly-symmetric reference object $s(\mathbf{x})$ has circular contours $\{\mathbf{x} : \; s(\mathbf{x}) = \text{constant}\}$. The object whose projections are measured is not necessarily circularly-symmetric; it is approximated by the function $d \cdot f(\mathbf{x})$, where $f(\mathbf{x})$ is an elongated object having elliptical contour lines. A circle can be deformed into an ellipse by linear coordinate transformation, and similarly, an appropriately chosen reference function $s(\mathbf{x})$ can be deformed into the

approximating object $f(\mathbf{x})$ by linear coordinate transformation, that is, $f(\mathbf{x}) = s(A\mathbf{x})$ where A is a 2×2 matrix. For our purposes, we consider coordinate transformations that can be represented as $A = A_3 A_2 A_1$, i.e., as the composite of up to three successive linear transformations:

1. Isotropic scaling of the coordinate system by a *size* factor R,

$$A_1 = \begin{bmatrix} \frac{1}{R} & 0 \\ 0 & \frac{1}{R} \end{bmatrix} \qquad 0 < R < \infty \tag{8}$$

2. Orthogonal stretching and compressing of the coordinate system to transform circular contours into ellipses with *eccentricity* (ratio of major to minor axes lengths) equal to λ,

$$A_2 = \begin{bmatrix} \frac{1}{\sqrt{\lambda}} & 0 \\ 0 & \sqrt{\lambda} \end{bmatrix} \qquad 1 < \lambda < \infty \tag{9}$$

3. Rotation of the coordinate system by the *orientation* angle ϕ,

$$A_3 = \begin{bmatrix} \cos\phi & \sin\phi \\ -\sin\phi & \cos\phi \end{bmatrix} \qquad -\frac{\pi}{2} \leq \phi < \frac{\pi}{2} \tag{10}$$

As an example of these transformations, consider the reference function $s(\mathbf{x})$ to be an indicator or characteristic function on a unit-radius disk centered on the origin. Then $d \cdot f(\mathbf{x}; R, \lambda, \phi)$, the object resulting from the composite of the three coordinate transformations in (8-10), is a function that is zero everywhere except on an ellipse centered at the origin, where it takes on the constant value d. Note that the reference function $s(\mathbf{x})$, or $s_p(r)$ in polar coordinates, is not restricted to being constant-valued; it may, for example, be a Gaussian object, $s_p(r) = \exp(-r^2)$.

Summarizing, the cross-section whose tomographic projections are measured is modeled as containing the object $d \cdot f(\mathbf{x}; R, \lambda, \phi)$, which is the result of linear coordinate transformation (scaling, stretching, and rotation) of a specified circularly-symmetric object $s(\mathbf{x})$. The focus of this paper is to evaluate how accurately the parameters characterizing size R, eccentricity λ, and orientation ϕ can be estimated from noisy tomographic data. A number of the results obtained in the remainder of this paper are expressed in terms of 2D Fourier transforms of

objects, particularly objects resulting from the scaling, stretching and/or rotation coordinate transformations in (8-10). For convenience, the relevant Fourier transform relationships [14] are summarized in Tables I and II.

The object $d \cdot f(\mathbf{x}; R, \lambda, \phi)$ resulting from the coordinate transformations has a Radon transform denoted by $d \cdot g(t, \theta; R, \lambda, \phi)$. As shown in Appendix 1, the energy of this Radon transform may be written in terms of ξ_s, the Radon transform energy of the symmetric reference object $s(\mathbf{x})$, as

$$\xi(d, R, \lambda) = d^2 \int_0^{\pi} \int_{-\infty}^{\infty} g^2(t, \theta; R, \lambda, \phi) dt d\theta = d^2 R^3 q(\lambda) \xi_s \tag{11}$$

The Radon transform energy depends on object eccentricity as

$$q(\lambda) = \frac{2}{\pi} \int_0^{\frac{\pi}{2}} \frac{1}{h(\lambda, \phi)} d\phi \tag{12}$$

where

$$h(\lambda, \varphi) \doteq [\lambda \cos^2 \varphi + \lambda^{-1} \sin^2 \varphi]^{1/2} \tag{13}$$

Note that $q(\lambda) = q(\lambda^{-1})$ and $q(1) = 1$; the Radon transform energy dependence on eccentricity $q(\lambda)$ is plotted in Figure 3.

IV. ML PARAMETER ESTIMATION

Let the noisy projection measurements be given by

$$y(t, \theta) = d \cdot g(t, \theta; R, \lambda, \phi) + w(t, \theta) \tag{14}$$

where measurements are taken at all points on the half-cylinder S defined in (4); $w(t, \theta)$ is a zero-mean white Gaussain noise process with spectral level $N_o/2$ [15]. The problem of characterizing the object geometry from noisy tomographic measurements may now be stated as: *given* noisy measurements of the Radon transform as shown in (14), *estimate* the object density d, size R, eccentricity λ, and orientation ϕ. It should be noted that, with the exception of the density factor d, these parameters enter the problem nonlinearly and lead to a nonlinear estimation problem of small dimensionality. This is in contrast to full image reconstruction, in which a linear estimation problem of high dimensionality is solved.

We consider now the problem of ML estimation of the three parameters R, λ, and ϕ that characterize the object's size, elongation and angular orientation. ML estimates of these

parameters are the values that maximize the log likelihood function [15]

$$L(R,\lambda,\phi;Y) = \frac{2d}{N_o}\int_0^\pi \int_{-\infty}^{\infty} y(t,\theta)g(t,\theta;R,\lambda,\phi)dtd\theta - \frac{d^2}{N_o}\int_0^\pi \int_{-\infty}^{\infty} g^2(t,\theta;R,\lambda,\phi)dtd\theta \quad (15)$$

The log likelihood function is the sum of two terms, the first of which is the result of 2D matched filtering of the measurements $y(t,\theta)$ with the Radon-space (i.e., (t,θ) coordinate system) filtering template $g(t,\theta;R,\lambda,\phi)$ and the second of which compensates for the energy in the Radon-space matched filtering template.

In order to compare the estimated and actual parameter values, let R_a, λ_a, ϕ_a denote the actual object parameters and $g(t,\theta;R_a,\lambda_a,\phi_a)$ the Radon transform of the actual object. The *ambiguity function*, or expected value of the log likelihood function, is given by

$$a(R,\lambda,\phi;R_a,\lambda_a,\phi_a) = \frac{2d^2}{N_o}\int_0^\pi \int_{-\infty}^{\infty} g(t,\theta;R_a,\lambda_a,\phi_a)g(t,\theta;R,\lambda,\phi)dtd\theta - \frac{d^2}{N_o}\int_0^\pi \int_{-\infty}^{\infty} g^2(t,\theta;R,\lambda,\phi)dtd\theta \quad (16)$$

As shown in Appendix 2, the ambiguity function depends on object size R only through the ratio R/R_a and depends on object orientation ϕ only through the difference $\Delta\phi \doteq \phi - \phi_a$. It may be written as the product of an SNR measure and a normalized ambiguity function,

$$a(R,\lambda,\phi;R_a,\lambda_a,\phi_a) = \frac{\xi_a}{N_o}a^*(R/R_a,\lambda,\lambda_a,\Delta\phi) \quad (17)$$

Here ξ_a is the energy in the Radon transform of the actual object, from (11)

$$\xi_a = d^2R_a^3q(\lambda_a)\xi_s \quad (18)$$

and the normalized ambiguity function is given by

$$a^*(R/R_a,\lambda,\lambda_a,\Delta\phi) = \frac{2}{q(\lambda_a)\xi_s}\left(\frac{R}{R_a}\right)^2\int_0^\pi \int_{-\infty}^{\infty} S_p\left(\rho h(\lambda_a,\psi)\right)S_p\left(\frac{\rho R}{R_a}h(\lambda,\psi+\Delta\phi)\right)d\rho d\psi - \frac{q(\lambda)}{q(\lambda_a)}\left(\frac{R}{R_a}\right)^3 \quad (19)$$

In this expression, $q(\cdot)$ is the Radon-space energy dependence on object eccentricity given in (12), and $S_p(r)$ is the Hankel transform of $s_p(r)$, i.e., a central section of the 2D Fourier transform of $s(\mathbf{x})$.

Since the parameter estimation problem being considered is nonlinear, the ambiguity function and log likelihood function are generally multimodal. Large measurement noise may therefore cause the ML estimates to occur at a likelihood function peak situated far from the true parameter values; in this case, the estimate has large error and is said to be *anomolous*. The probability of obtaining an anomolous estimate may be characterized from knowledge of the ambiguity function [9,10,15], and becasue of this the ambiguity function plays a key role in assessing ML estimation performance. The ambiguity function also plays a key role in assessing *local* estimation performance, that is, in identifying the estimate error variance in the case when the estimate is not anomolous and occurs close to the true parameter value. In this case, estimation performance may be characterized by employing a linearized error analysis which leads to the CRLB on the error variance. Computationally, the CRLB is obtained by evaluating the inverse of the second partial derivative of the ambiguity function [15]. In what follows, we focus on characterizing this bound on the local error variance which is relevant in the case of moderate to small noise levels.

The expressions developed thus far apply for an arbitrary choice of the circularly-symmetric reference object $s_p(r)$. In the following section, the problem of ML geometry estimation is examined in more detail for the analytically tractable case of Gaussian objects. Furthermore, to simplify the interpretation and develop insight into the problem of estimating object geometry from tomographic data, the three-parameter problem is considered as three separate subproblems with one parameter unknown at a time. The object size estimation problem is considered first in which the object is taken to be circularly-symmetric ($\lambda = \lambda_a = 1$ and $\Delta\phi$=0). The eccentricity estimation problem is then considered in which the size and orientation are taken to be known ($R = R_a$ and $\Delta\phi$=0). Finally, the orientation estimation problem is considered in which object size and eccentricity are assumed to be known ($R = R_a$ and $\lambda = \lambda_a$).

V. GAUSSIAN OBJECT

The log likelihood and ambiguity functions presented in the previous section are evaluated in this section for the case of Gaussian objects (see [9] for some extensions to more general objects). Begin with the circularly-symmetric *Gaussian* reference object

$$s_g(r) = \exp(-r^2) \tag{20}$$

The Hankel transform of $s_g(r)$ is

$$S_g(\rho) = \pi \exp(-\pi^2 \rho^2) \tag{21}$$

and the energy in the Radon transform of $s_g(r)$ is

$$\xi_g = \sqrt{\pi/2}\, \pi^2 \tag{22}$$

By substituting (21) and (22) into (19), and noting that

$$\int_0^\infty e^{-a^2\rho^2} d\rho = \frac{\sqrt{\pi}}{2a} \tag{23}$$

an expression is obtained for the Gaussian object normalized ambiguity function

$$a^*(R/R_a, \lambda, \lambda_a, \Delta\phi) = \frac{2\sqrt{2}}{q(\lambda_a)} \left(\frac{R}{R_a}\right)^2 \left[\frac{1}{\pi} \int_0^\pi \left\{h^2(\lambda_a, \psi) + (R/R_a)^2 h^2(\lambda, \psi + \Delta\phi)\right\}^{-1/2} d\psi\right] - \frac{q(\lambda)}{q(\lambda_a)} \left(\frac{R}{R_a}\right)^3 \tag{24}$$

Size Estimation

Consider first the problem of using noisy full-view projection measurements to estimate the size of a Gaussian object that results from isotropic coordinate scaling (the coordinate transformation A_1 in (8)) of the circularly-symmetric Gaussian reference object. The size estimation ambiguity function for this case is given by

$$a(R, R_a) = \left(\frac{\xi_a}{N_o}\right) a^*(R/R_a) \tag{25}$$

where ξ_a is the actual object Radon transform energy $d^2 R_a^3 \xi_g$ and $a^*(R/R_a)$ is the special case of the normalized ambiguity function in (24) when $\lambda = \lambda_a = 1$ and $\Delta\phi = 0$. The normalized ambiguity function is plotted in Figure 4 along with the normalized ambiguity function for the case of a *disk* object (everywhere zero except on a disk of radius R_a, where it takes on a constant value). The close resemblance of these two curves indicates that the ambiguity function for object size estimation is not sensitive to the detailed density variations within the object boundary. Furthermore, these two ambiguity functions attain their maximum value at the true size $R = R_a$ and decrease monotonically and relatively rapidly away from this point. Qualitatively, this suggests good estimation performance, since the peak will not shift significantly with the addition of a small amount of noise.

The CRLB on the size estimate error variance is obtained by evaluating the second partial derivative of the ambiguity function with respect to the parameter R. The normalized CRLB on the size estimate error variance is derived in Appendix 3 and is given by

$$\left(\frac{\sigma_R}{R_a}\right)^2 \geq \frac{2}{11}\frac{N_o}{\xi_a} \tag{26}$$

This bound on the relative error in the size estimate is simply a constant divided by the SNR. From (18), the Radon space signal energy varies as d^2R^3, so two objects with different sizes but the same value of d^2R^3 are characterized by the same relative error variance of the size estimate. Since signal energy depends on the third power of size R, relative size estimation error variance decreases very rapidly with object size.

Eccentricity Estimation

Consider now the problem of estimating the eccentricity of a Gaussian object, assuming that all other details such as location, size and orientation are known *a priori*. For a circularly-symmetric Gaussian object of known size R_a which is elongated by undergoing the coordinate transformation in (9) with an unknown eccentricity factor λ_a, the eccentricity estimation ambiguity function is

$$a(\lambda, \lambda_a) = \frac{\xi_a}{N_o} a^*(\lambda, \lambda_a) \tag{27}$$

Here ξ_a is the actual object Radon transform energy $d^2R_a^3 q(\lambda_a)\xi_g$ and $a^*(\lambda, \lambda_a)$ is the special case of the normalized ambiguity function in (24) where $R_a = R$ and $\Delta\phi = 0$, which can be reduced to the expression

$$a^*(\lambda, \lambda_a) = \frac{2\sqrt{2}\sqrt[4]{\lambda\lambda_a}\, q(\sqrt{\lambda\lambda_a})}{\sqrt{\lambda + \lambda_a}\, q(\lambda_a)} - \frac{q(\lambda)}{q(\lambda_a)} \tag{28}$$

Figure 5 is a plot of this expression when the actual object eccentricity λ_a is equal to 4. The peak of the ambiguity function occurs at the true parameter value, however, the function does not decrease rapidly away from the true value. This suggests that accurate estimation of object eccentricity requires a high measurement SNR, even when all other parameters are known perfectly.

The CRLB on the error variance of the eccentricity estimate is obtained by taking the second derivative of the ambiguity function with respect to λ; the normalized CRLB is

given by

$$\left(\frac{\sigma_\lambda}{\lambda_a}\right)^2 \geq \frac{8N_o}{3d^2R_a^3\lambda_a^2\xi_g}\left\{\frac{2}{\pi}\int_0^{\pi/2}[h(\lambda_a,\psi)]^{-5/2}\left(\cos^2\psi-\frac{1}{\lambda_a^2}\sin^2\psi\right)^2 d\psi\right\}^{-1}$$
$$\approx \frac{4}{3}q(\lambda_a)\frac{N_o}{\xi_a} = \frac{4}{3d^2R_a^3}\frac{N_o}{\xi_g} \qquad \lambda_a \in [1,20] \tag{29}$$

where the last line is obtained by numerical evaluation [9]. The lower bound on the relative error variance in the eccentricity estimate is essentially a constant times $q(\lambda_a)$ divided by the SNR. For a fixed noise level N_o, all objects with the same value of $d^2R_a^3$ have the same normalized eccentricity estimate error variance, regardless of their eccentricity, i.e., relative eccentricity error variance does *not* decrease as the object becomes more eccentric.

Orientation Estimation

Consider finally the problem of estimating the angular orientation of an elongated Gaussian object from noisy full-view projection measurements. For a circularly-symmetric Gaussian object of known size R_a which undergoes the eccentricity coordinate transformation in (9) with a known eccentricity factor λ_a, and then undergoes the rotation coordinate transformation in (10) with an unknown rotation angle ϕ, the orientation estimation ambiguity function is

$$a(\Delta\phi) = \frac{\xi_a}{N_o}a^*(\Delta\phi) \tag{30}$$

Here ξ_a is the ϕ-independent actual object Radon transform energy $d^2R_a^3q(\lambda_a)\xi_g$, and $a^*(\Delta\phi)$ is the special case of the normalized ambiguity function in (24) where $R = R_a$ and $\lambda = \lambda_a$. Note that $a^*(\Delta\phi)$ is symmetric in $\Delta\phi$ (because the eccentric object is centrally-symmetric or balanced), and $a^*(\Delta\phi,\lambda_a) = a^*(\Delta\phi,\lambda_a^{-1})$, since these are ambiguity functions for the same object rotated by 90 degrees. The normalized orientation ambiguity function is plotted in Figure 6 for several values of actual object eccentricity λ_a. Narrow objects have a more sharply peaked orientation ambiguity function, qualitatively confirming the intuitive notion that the estimation of orientation is more reliable for eccentric as compared to nearly circular objects.

This may be expressed more precisely by evaluating the CRLB on the orientation estimate error variance, which may be calculated as the inverse of the second partial derivative of the ambiguity function,

$$\sigma^2_{\Delta\phi} \geq \frac{N_o}{\xi_a} q(\lambda_a) \left\{ \frac{3}{8} (\lambda_a^{-1} - \lambda_a)^2 \left[\frac{2}{\pi} \int_0^{\pi/2} h(\lambda_a, \psi)^{-5/2} \sin^2(2\psi) d\psi \right] + (\lambda_a^{-1} - \lambda_a) \left[\frac{2}{\pi} \int_0^{\pi/2} h(\lambda_a, \psi)^{-3/2} \cos(2\psi) d\psi \right] \right\}^{-1}$$

$$\doteq \frac{N_o}{d^2 R^3 \xi_g} \Upsilon(\lambda_a) \tag{31}$$

$\Upsilon(\lambda_a)$, the dependence of the error variance bound on object eccentricity is plotted in Figure 7. The bound is seen to be a rapidly decreasing function of eccentricity, which is expected, since it is easier to estimate the orientation of more eccentric objects. The CRLB, then, is a decreasing function of both SNR and object eccentricity; this suggests the possibility of adapting the model complexity (number parameters or degrees of freedom) to the measurement quality, which is explored in the following section.

Selecting the Modeled Object Complexity

Figure 7 confirms the intuitive notion that the estimate of the angular orientation of the object improves as the object becomes increasingly elongated and with increasing SNR. Conversely, for values of λ_a approaching unity (object contours nearly circular) the bound approaches infinity, that is, a very high SNR is required to estimate the orientation. However, in the case of a nearly circular object, orientation is a far less important parameter than say object size, which could in this case be determined by using a simpler circularly-symmetric object model. Here, we turn this intuitive notion into a precise decision rule for selecting, based on knowledge of the SNR $d^2 R^3 \xi_g / N_o$ and an estimate of object eccentricity $\hat{\lambda}$, between the following two hypotheses:

H_0: the object is nearly circularly-symmetric ($\lambda \approx 1$)

H_1: the object has an elongated geometry ($\lambda > 1$)

Various criteria may be used to develop a decision rule for these hypotheses, and our criterion is based on the observation that if the available measurements do not provide a high quality orientation estimate (i.e., the error variance is too large), it is more appropriate to assume that the object is circularly-symmetric. In particular, suppose that an *a priori* limit κ

exists on the maximum acceptable value of orientation estimate error variance $\sigma^2_{\Delta\phi}$. The decision rule we propose is to decide H_1 if and only if the bound on the error variance of the orientation estimate does not exceed κ, that is, decide H_1 if and only if:

$$\frac{N_o}{d^2 R^3 \xi_g} \Upsilon(\hat{\lambda}) < \kappa \tag{32}$$

or

$$\Upsilon(\hat{\lambda}) < \frac{d^2 R^3 \xi_g}{N_o} \kappa \tag{33}$$

or, since $\Upsilon(\lambda)$ is a monotonically decreasing function,

$$\hat{\lambda} > \Upsilon^{-1} \left\{ \frac{d^2 R^3 \xi_g}{N_o} \kappa \right\} \doteq \lambda_{min}(\text{SNR}, \kappa) \tag{34}$$

Thus, given a minimum acceptable orientation error variance κ and knowing the measurement SNR, the rule in (34) may be employed to decide, based on the estimated eccentricity $\hat{\lambda}$, whether to use an elliptical model (with a corresponding orientation estimate meeting the accuracy specification κ) or, because sufficient orientation accuracy cannot be insured, to use a simpler circularly symmetric model.

VI. CONCLUSIONS

The problem has been considered of estimating the size, eccentricity and orientation of an object within a cross-section of a 2D medium from noisy tomographic data, i.e., noisy observations of the Radon transform. The object in the cross-section has been modeled as the result of applying one or more of the linear coordinate transformations in (8-10) to a circularly-symmetric reference object, with the coordinate transformations parameterized by three variables corresponding to object size, eccentricity and orientation. ML estimation of these parameters was investigated via evaluation of the ambiguity function and the CRLB on the estimate error variance, and results were illustrated for the class of Gaussian objects. It was demonstrated that for measurements available at all projection angles and at a given noise level, (1) object size and orientation can be estimated more accurately than the degree of object elongation, and (2) reliable orientation estimation requires a minimum degree of object elongation, and the required degree of elongation is inversely related to the measurement SNR. This result was used to derive a simple decision rule for selecting the appropriate complexity of the modeled object (circular versus elongated).

Extensions of some of these results to noncircularly symmetric objects may be found in [9]. Also in [9] may be found a discussion of the robustness of the ML geometry estimation procedure discussed in this paper, including robustness to modeling errors such as incorrect choice of reference object $s(\mathbf{x})$ and incorrect knowledge of the object location. Generally, geometry parameter estimation has been found to be quite robust to a variety of modelling errors.

APPENDIX 1 – Radon-space Energy of an Eccentric Object

The Radon-space energy $\xi(d,R,\lambda)$ in (11), which is independent of the object orientation parameter ϕ, is given by

$$\xi(d,R,\lambda) = d^2 \int_0^{\pi} \int_{-\infty}^{\infty} g^2(t,\theta;R,\lambda,\phi)\, dt\, d\theta \tag{35}$$

By the definition of the back-projection operator defined in (5), this may be written as

$$\xi(d,R,\lambda) = d^2 \left[\mathbf{B}(g \star g)\right](\mathbf{x})\,|_{\mathbf{x}=\mathbf{0}} \tag{36}$$

where $\star$ denotes 1D convolution in the t variable. Noting that g is the Radon transform of f as defined in (1),

$$\begin{aligned} \xi(d,R,\lambda) &= d^2 \left[\mathbf{B}(\mathbf{R}f \star \mathbf{R}f)\right](\mathbf{x})\,|_{\mathbf{x}=\mathbf{0}} \\ &= d^2 \left[f \star\star f \star\star \frac{1}{|\,r\,|}\right](\mathbf{x})\,|_{\mathbf{x}=\mathbf{0}} \end{aligned} \tag{37}$$

where $\star\star$ denotes 2D convolution, and the last line follows from repeated application of the equality [10,16]

$$\left[\mathbf{B}(\mathbf{R}f \star \nu)\right](\mathbf{x}) = \left[f \star\star \mathbf{B}\nu\right](\mathbf{x}) \tag{38}$$

That is, CBP of $[\mathbf{R}f](t,\theta)$ with convolving kernel $\nu(t,\theta)$ may be written as the 2D convolution of $f(\mathbf{x})$ with the back-projection of $\nu(t,\theta)$.

Denoting the 2D inverse Fourier transform as $F_2^{-1}\{\cdot\}$, (37) may be written as

$$\begin{aligned} \xi(d,R,\lambda) &= d^2 \left[F_2^{-1}\left\{F_p^2(\rho,\psi)\frac{1}{|\,\rho\,|}\right\}\right](\mathbf{x})\,|_{\mathbf{x}=\mathbf{0}} = d^2 \int_0^{\pi} \int_{-\infty}^{\infty} F_p^2(\rho,\psi) d\rho d\psi \\ &= d^2 R^4 \int_0^{\pi} \int_{-\infty}^{\infty} S_p^2\left(R\,\rho\,h(\lambda,\psi)\right) d\rho\, d\psi \end{aligned} \tag{39}$$

The last line follows because $f(\mathbf{x})$ is the result of applying the scaling and stretching transformations in (8-10) to the circularly-symmetric object $s(\mathbf{x})$, and from Table II and $h(\lambda,\psi)$ defined in (13),

$$F_p(\rho,\psi) = R^2 S_p\left(R\,\rho\,h(\lambda,\psi)\right) \tag{40}$$

Note that from (39) the Radon space energy ξ_s of the reference object $s_p(\rho)$ is

$$\xi_s = \xi(1,1,1) = \int_0^{\pi} \int_{-\infty}^{\infty} S_p^2(\rho)\, d\rho\, d\psi = \pi \int_{-\infty}^{\infty} S_p^2(\rho)\, d\rho \tag{41}$$

Now by a change of variable, (39) may be written as

$$\xi(d,R,\lambda) = d^2R^3 \int_0^{\pi} \{h(\lambda,\psi)\}^{-1}\, d\psi \int_{-\infty}^{\infty} S_p^2(\rho)\, d\rho \;=\; d^2R^3 q(\lambda)\xi_s \tag{42}$$

where $q(\lambda)$ is defined in (12).

APPENDIX 2 – Geometry Parameter Ambiguity Function

To simplify the notation, let the subscripts a and m correspond to the actual object (characterized by R_a, λ_a, ϕ_a) and modeled object (characterized by R, λ, ϕ), respectively. The ambiguity function in (16) may then be expressed as

$$a(R,\lambda,\phi;R_a,\lambda_a,\phi_a) = \frac{2d^2}{N_o}\int_0^{\pi}\int_{-\infty}^{\infty} g_a(t,\theta)g_m(t,\theta)\,dt\,d\theta - \frac{d^2}{N_o}\int_0^{\pi}\int_{-\infty}^{\infty} g_m^2(t,\theta)\,dt\,d\theta \quad (43)$$

The first term may be interpreted as a convolution back-projection operation (equation (5)) evaluated at the origin, and the second term may be rewritten using (11),

$$\begin{aligned} a(R,\lambda,\phi;R_a,\lambda_a,\phi_a) &= \frac{2d^2}{N_o}\mathbf{B}\left[g_a \star g_m\right](\mathbf{x})\,|_{\mathbf{x}=\mathbf{0}} - \frac{d^2}{N_o}R^3 q(\lambda)\xi_s \\ &= \frac{2d^2}{N_o}\mathbf{B}\left[\mathbf{R}f_a \star \mathbf{R}f_m\right](\mathbf{x})\,|_{\mathbf{x}=\mathbf{0}} - \frac{\xi_a}{N_o}\left[\frac{q(\lambda)}{q(\lambda_a)}\left(\frac{R}{R_a}\right)^3\right] \end{aligned} \quad (44)$$

where $\mathbf{R}$ and $\mathbf{B}$ denote the Radon transformation and back-projection operators in (1) and (5), $\star$ denotes 1D convolution with respect to the t variable, and the actual object energy ξ_a is given in (18). Using the equality in (38), denoting the 2D inverse Fourier transform by $F_2^{-1}\{\cdot\}$, and letting $F_a(\rho,\psi)$ and $F_m(\rho,\psi)$ denote the 2D Fourier transform of the actual and modeled objects in polar coordinates,

$$\begin{aligned} &a(R,\lambda,\phi;R_a,\lambda_a,\phi_a) \\ &= \frac{2d^2}{N_o}\left[f_a \star\star f_m \star\star \frac{1}{|r|}\right](\mathbf{x})\,|_{\mathbf{x}=\mathbf{0}} - \frac{\xi_a}{N_o}\left[\frac{q(\lambda)}{q(\lambda_a)}\left(\frac{R}{R_a}\right)^3\right] \\ &= \frac{2d^2}{N_o}\left[F_2^{-1}\left\{F_a(\rho,\psi)F_m(\rho,\psi)\frac{1}{|\rho|}\right\}\right](\mathbf{x})\,|_{\mathbf{x}=\mathbf{0}} - \frac{\xi_a}{N_o}\left[\frac{q(\lambda)}{q(\lambda_a)}\left(\frac{R}{R_a}\right)^3\right] \\ &= \frac{2d^2}{N_o}\int_0^{\pi}\int_{-\infty}^{\infty} F_a(\rho,\psi)F_m(\rho,\psi)d\rho\,d\psi - \frac{\xi_a}{N_o}\left[\frac{q(\lambda)}{q(\lambda_a)}\left(\frac{R}{R_a}\right)^3\right] \end{aligned} \quad (45)$$

The actual and modeled objects are obtained from the circularly-symmetric object $s(\mathbf{x})$ (or $s_p(r)$ in polar coordinates) with 2D Fourier transform $S(\omega)$ (or $S_p(\rho)$ in polar coordinates) by application of the coordinate transformations in (8-10). Using the Fourier transform relationships in Table II,

$$\begin{aligned} &a(R,\lambda,\phi;R_a,\lambda_a,\phi_a) \\ &= \frac{2d^2}{N_o}\int_0^{\pi}\int_{-\infty}^{\infty} R_a^2 S_p\left(\rho\,R_a\,h(\lambda_a,\psi+\phi_a)\right)\,R^2 S_p\left(\rho\,R\,h(\lambda,\psi+\phi)\right)\,d\rho d\psi \\ &\qquad - \frac{\xi_a}{N_o}\left[\frac{q(\lambda)}{q(\lambda_a)}\left(\frac{R}{R_a}\right)^3\right] \end{aligned}$$

$$= \frac{\xi_a}{N_o}\left[\frac{2}{q(\lambda_a)\xi_s}\left(\frac{R}{R_a}\right)^2\right]\int_0^{\pi}\int_{-\infty}^{\infty} S_p\left(\rho\, h(\lambda_a,\psi)\right) S_p\left(\frac{\rho R}{R_a}\, h(\lambda,\psi+\phi-\phi_a)\right) d\rho d\psi$$
$$-\frac{\xi_a}{N_o}\left[\frac{q(\lambda)}{q(\lambda_a)}\left(\frac{R}{R_a}\right)^3\right] \tag{46}$$

where the last line follows by a change of variable.

APPENDIX 3 – Size Estimate Cramer-Rao Bound

Consider an arbitrary (not necessarily Gaussian) circularly-symmetric object $s_p(r)$ with Hankel transform $S_p(\rho)$. The size estimation ambiguity function is the special case of (17)-(19) where $\lambda = \lambda_a = 1$ and $\Delta\phi = 0$,

$$a(R, R_a) = \frac{2\xi_a}{\xi_s N_o} \int_0^{2\pi} \int_0^{\infty} S_p(\rho) S_p\left(\frac{\rho R}{R_a}\right) d\rho d\psi \; - \; \frac{\xi_a}{N_o}\left(\frac{R}{R_a}\right)^3 \tag{47}$$

Let the first two partial derivatives of $S_p(\rho)$ with respect to ρ be denoted by $S_p'(\rho)$ and $S_p''(\rho)$. The second partial derivative of $a(R, R_a)$ in (47) is given by

$$\frac{\partial^2 a(R, R_a)}{\partial R^2} =$$
$$\frac{\xi_a}{N_o}\left[\frac{4\pi}{\xi_s}\left(\frac{R}{R_a}\right)^2 \int_0^{\infty} \left(\frac{\rho}{R_a}\right)^2 S_p(\rho) S_p''\left(\frac{\rho R}{R_a}\right) d\rho + \frac{16\pi R}{\xi_s R_a^2} \int_0^{\infty} \left(\frac{\rho}{R_a}\right) S_p(\rho) S_p'\left(\frac{\rho R}{R_a}\right) d\rho \right.$$
$$\left. + \frac{8\pi}{\xi_s R_a^2} \int_0^{\infty} S_p(\rho) S_p\left(\frac{\rho R}{R_a}\right) d\rho \; - \; \frac{6R}{R_a^3}\right] \tag{48}$$

The CRLB on the size estimate error variance may then be written as

$$\sigma_R^2 \geq \left[\left\{\frac{\partial^2 a(R, R_a)}{\partial R^2}\right\}_{R=R_a}\right]^{-1} = \frac{N_o}{2d^2 R_a (3\xi_s - \varsigma)} \tag{49}$$

where

$$\varsigma \doteq 2\pi \int_0^{\infty} S_p(\rho)\left[2S_p(\rho) + 4\rho S_p'(\rho) + \rho^2 S_p''(\rho)\right] d\rho \tag{50}$$

For the special case of the Gaussian object in (20), ς in (50) equals $(\pi/2)^{2.5}$, $\xi_s = \xi_g$ in (22) and the CRLB becomes

$$\sigma_R^2 \geq \left(\frac{2}{\pi}\right)^{2.5}\left[\frac{N_o}{22\, d^2 R_a}\right] \tag{51}$$

or after normalizing,

$$\left(\frac{\sigma_R}{R_a}\right)^2 \geq \frac{2}{11}\frac{N_o}{\xi_a} \tag{52}$$

where $\xi_a = d^2 R_a^3\, \xi_g$ is the actual object Radon transform energy in (18).

AFFILIATION OF AUTHORS

[1] E.P. Schlumberger, 26 rue de la Cavée, 92140 CLAMART, France

[2] Dept. of E.E.C.S., MIT, Room 35-233, Cambridge, MA 02139, USA

This work was supported by the National Science Foundation under Grant ECS-8312921.

REFERENCES

[1] B. Cornuelle, "Acoustic Tomography," *IEEE Trans. Geoscience and Remote Sensing,* vol. GE-20, pp. 326-332, July 1982.

[2] R. Guzzardi, G. Licitra and M. R. Voegelin, "Recent developments in Compton tomographic imaging of the lung and possible application to object recognition," *IEEE Trans. Nuclear Sci.*, vol. NS-34, pp. 667-671, June 1987.

[3] R. J. Lytle and M. R. Portnoff, "Detecting high-contrast seismic anomolies using cross-borehole probing," *IEEE Trans. Geoscience and Remote Sensing,* vol. GE-22, pp. 93-98, March 1984.

[4] Special Section on Geotomography, *Proc. IEEE*, vol. 74, pp. 328-360, Feb. 1986.

[5] Special Issue on Computerized Tomography, *Proc. IEEE*, vol. 71, pp. 291-431, March 1983.

[6] R. L. Parker, "Understanding inverse theory," *Ann. Rev. Earth Planet. Sci.*, vol. 5, pp. 35-64, 1977.

[7] T. Tomitani, "An edge detection algorithm for attenuation correction emission CT," *IEEE Trans. Nuclear Sci.*, Vol. NS-34, pp. 309-312, Feb. 1987.

[8] D. L. Snyder, "Utilizing side information in emission tomography," *IEEE Trans. Nuclear Sci.*, Vol. NS-31, pp. 533-537, Feb. 1984.

[9] D. Rossi, "Reconstruction from projections based on detection and estimation of objects," Ph.D. Dissertation, Department of Electrical Engineering and Computer Science, M.I.T., Cambridge, August 1982.

[10] D. Rossi and A. Willsky, "Reconstruction from projections based on detection and estimation of objects," *IEEE Trans. Acoust., Speech, and Signal Proc.*, vol. ASSP-32, pp. 886-906, August 1984.

[11] S. W. Rowland, "Computer implementation of image reconstruction formulas," in *Image Reconstruction from Projections - Implementation and Applications* (Topics in Applied Physics, vol. 32), G.T. Herman, Ed. New York: Springer-Verlag, 1979.

[12] L. A. Santalo, *Integral Geometry and Geometric Probability.* Encyclopedia of mathematics and its applications I, G. Rota, Ed. Reading, MA: Addison-Wesley, 1976.

[13] D. B. Cooper, H. Elliott, F. Cohen, L. Reiss, and P. Symosek, "Stochastic boundary estimation and object recognition." *Computer Graphics and Image Processing,* vol. 12, pp. 326-356, 1980.

[14] R. Bracewell, *The Fourier Transform and its Applications.* New York: McGraw-Hill, 1965.

[15] H. Van Trees, *Detection, Estimation, and Modulation Theory, Part I,* New York: Wiley, 1968.

[16] M. E. Davison, F. A. Grunbaum, "Tomographic reconstruction with arbitrary directions." *Comm. in Pure and Appl. Math.*, vol. 34, pp. 77-120, 1981.

Table I – Coordinate Transformations in the Spatial Domain

	Cartesian Coordinates	Polar Coordinates
Original Function	$s(x_1, x_2)$	$s_p(r, \varphi)$
Size Transformation A_1 in (8)	$s(x_1/R, x_2/R)$	$s_p(r/R, \varphi)$
Eccentricity Transformation* A_2 in (9)	$s(x_1/\sqrt{\lambda}, \sqrt{\lambda}\, x_2)$	$s_p\left(r\, h^{-1}(\lambda, \varphi), \tan^{-1}(\lambda \tan \varphi)\right)$
Orientation Transformation A_3 in (10)	$s(x_1 \cos\phi + x_2 \sin\phi, -x_1 \sin\phi + x_2 \cos\phi)$	$s_p(r, \varphi - \phi)$

Table II – Coordinate Transformations in the Frequency Domain

	Cartesian Coordinates	Polar Coordinates
Original Function	$S(\omega_1, \omega_2)$	$S_p(\rho, \psi)$
Size Transformation A_1 in (8)	$R^2 S(R\omega_1, R\omega_2)$	$R^2 S_p(R\rho, \psi)$
Eccentricity Transformation* A_2 in (9)	$S\left(\sqrt{\lambda}\,\omega_1, \omega_2/\sqrt{\lambda}\right)$	$S_p\left(\rho\, h(\lambda, \psi), \tan^{-1}\left(\frac{1}{\lambda}\tan\psi\right)\right)$
Orientation Transformation A_3 in (10)	$S(\omega_1 \cos\phi + \omega_2 \sin\phi, -\omega_1 \sin\phi + \omega_2 \cos\phi)$	$S_p(\rho, \psi + \phi)$

* $h(\lambda, \varphi) \doteq \left(\lambda \cos^2\varphi + \lambda^{-1} \sin^2\varphi\right)^{1/2}$

Figure Captions

Fig. 1. Projection at angle θ.

Fig. 2. Measurement geometry.

Fig. 3. Radon transform energy dependence on eccentricity λ.

Fig. 4. Size ambiguity functions for Gaussian and disk objects.

Fig. 5. Normalized eccentricity ambiguity function; $\lambda_a = 4$.

Fig. 6. Orientation ambiguity function for a Gaussian object for several values of eccentricity.

Fig. 7. Normalized orientation Cramer-Rao bound.

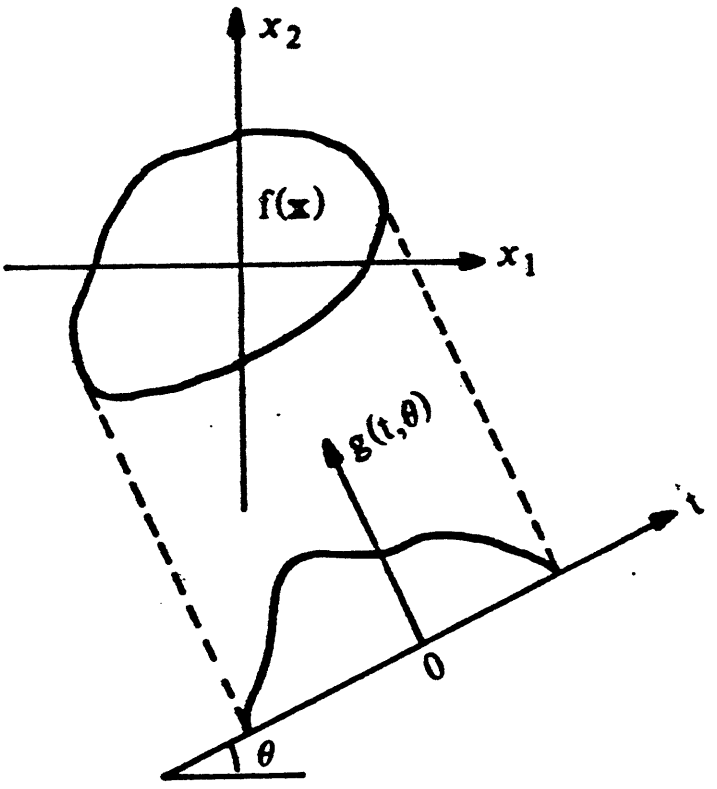

Fig. 1. Projection at angle θ.

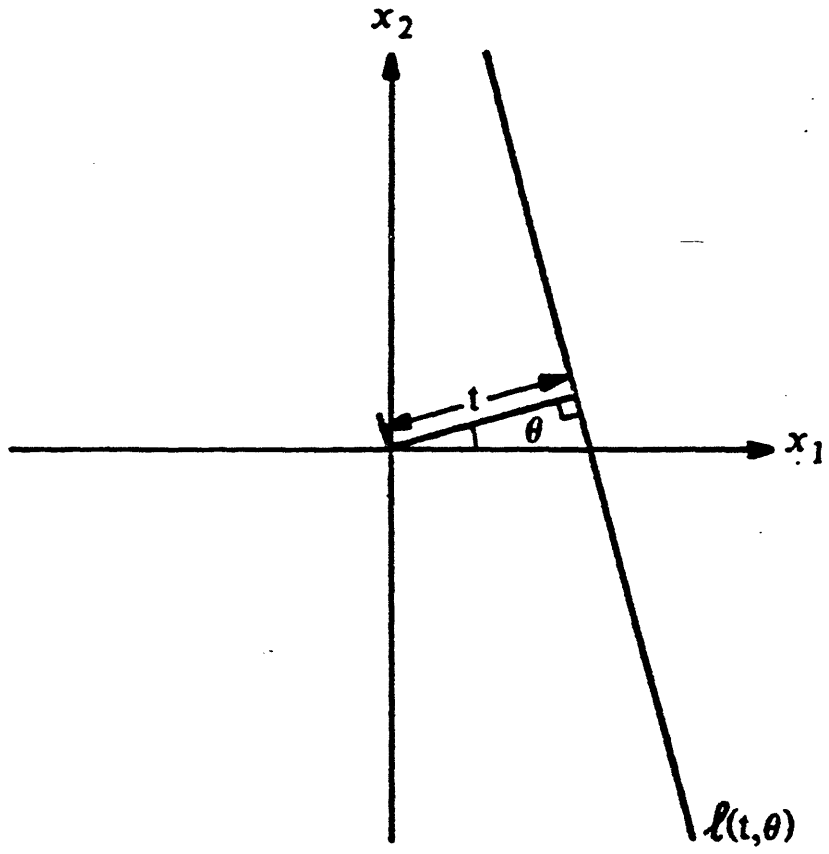

Fig. 2. Measurement geometry.

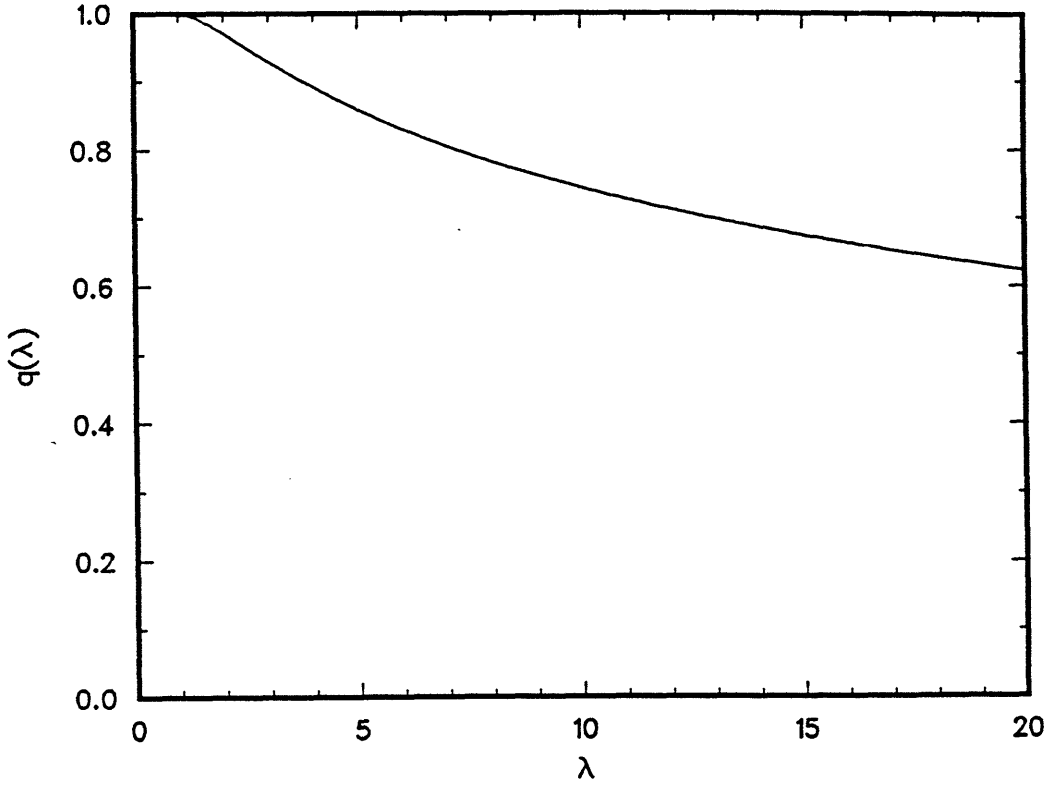

Fig. 3. Radon transform energy dependence on eccentricity λ.

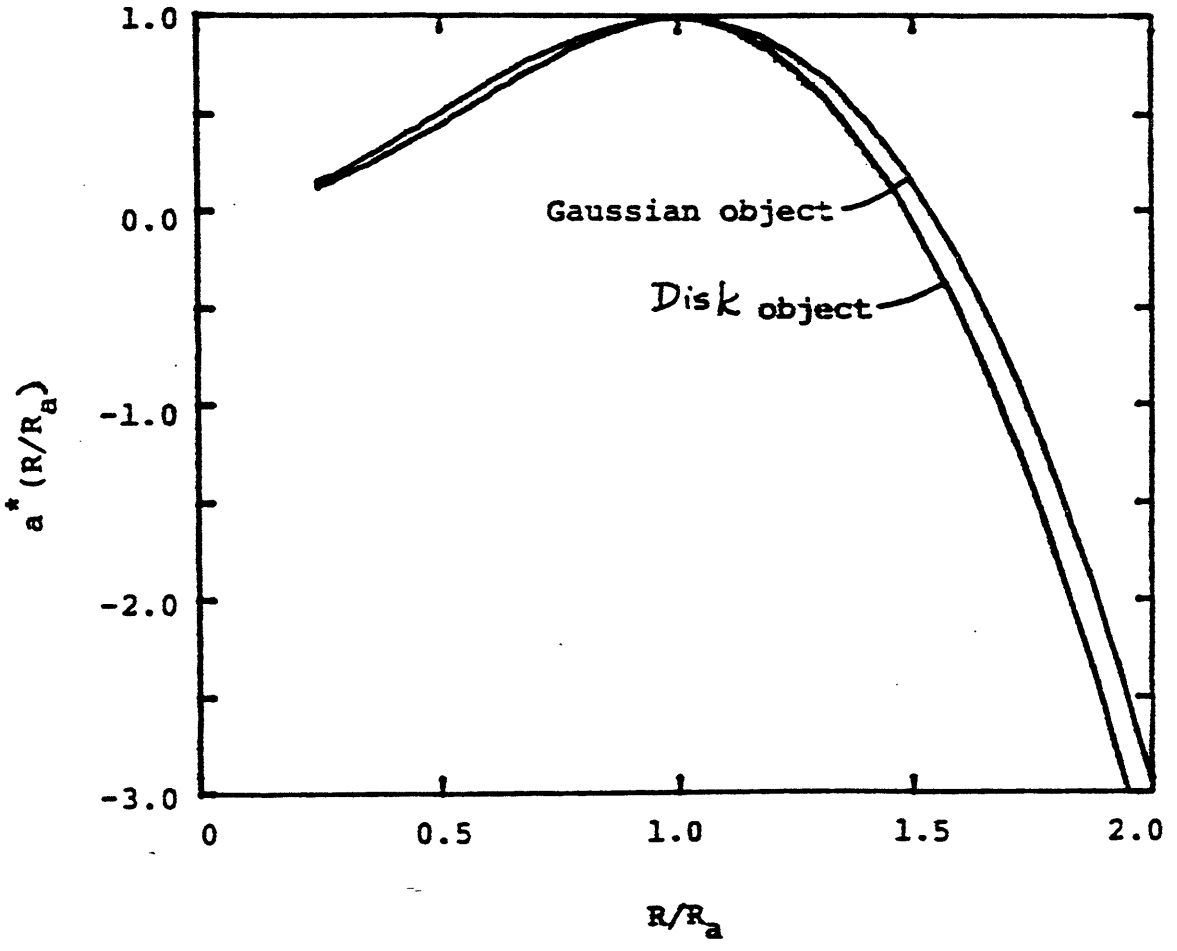

Fig. 4. Size ambiguity functions for Gaussian and disk objects.

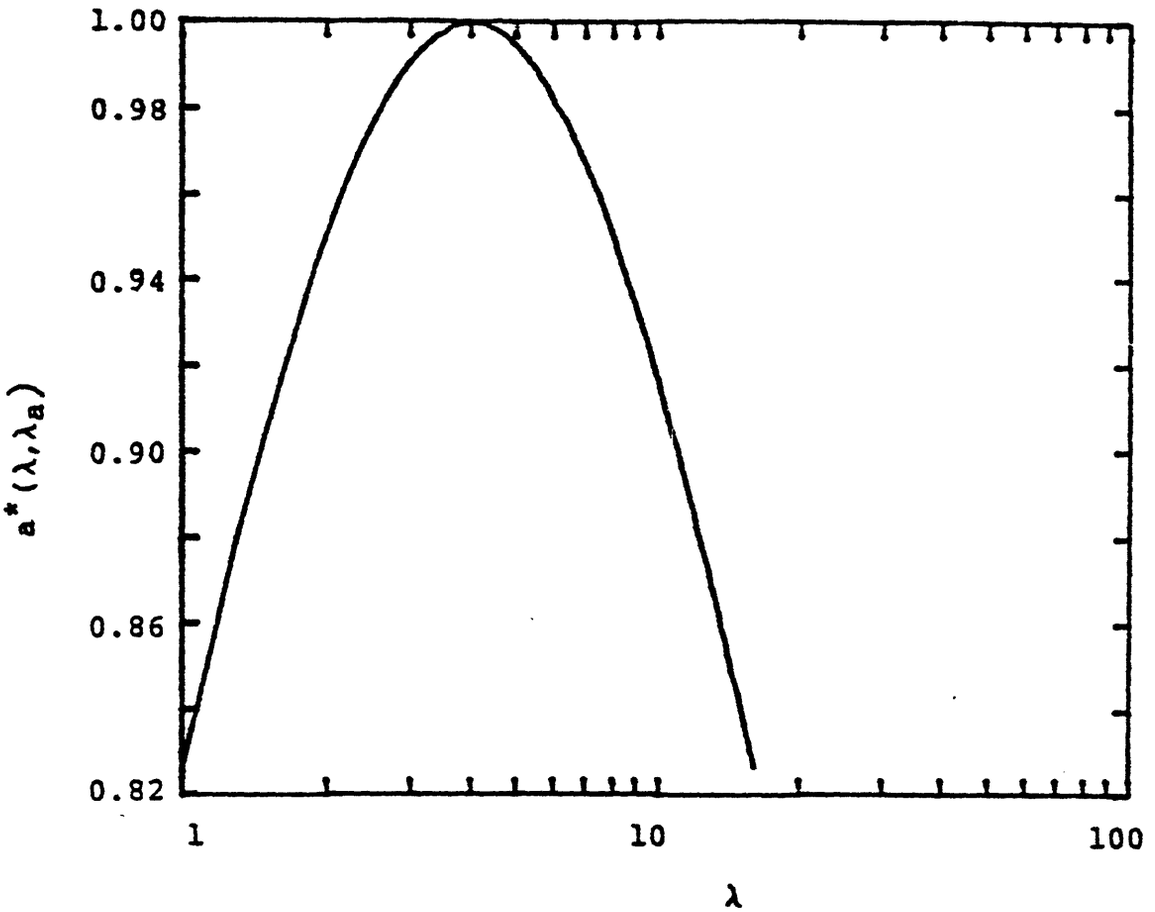

Fig. 5. Normalized eccentricity ambiguity function; $\lambda_a = 4$.

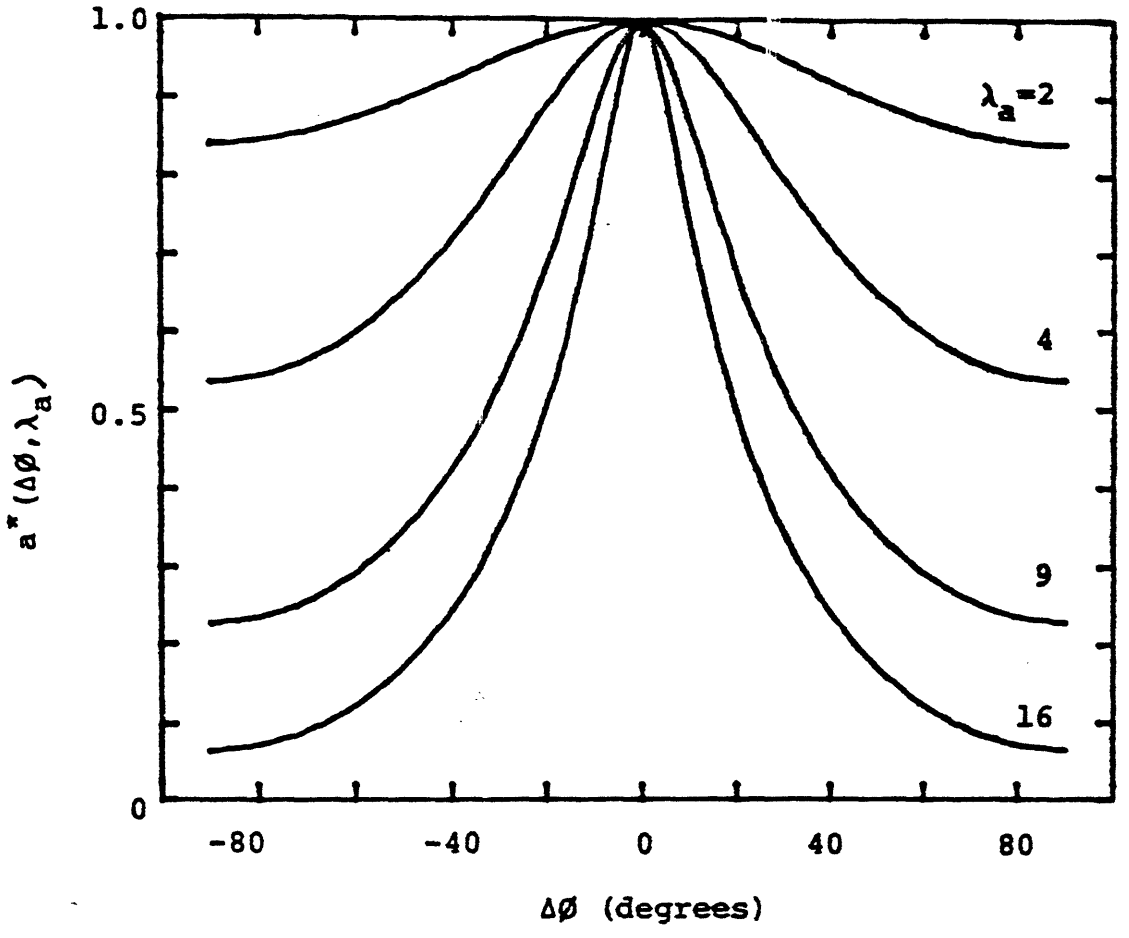

Fig. 6. Orientation ambiguity function for a Gaussian object for several values of eccentricity.

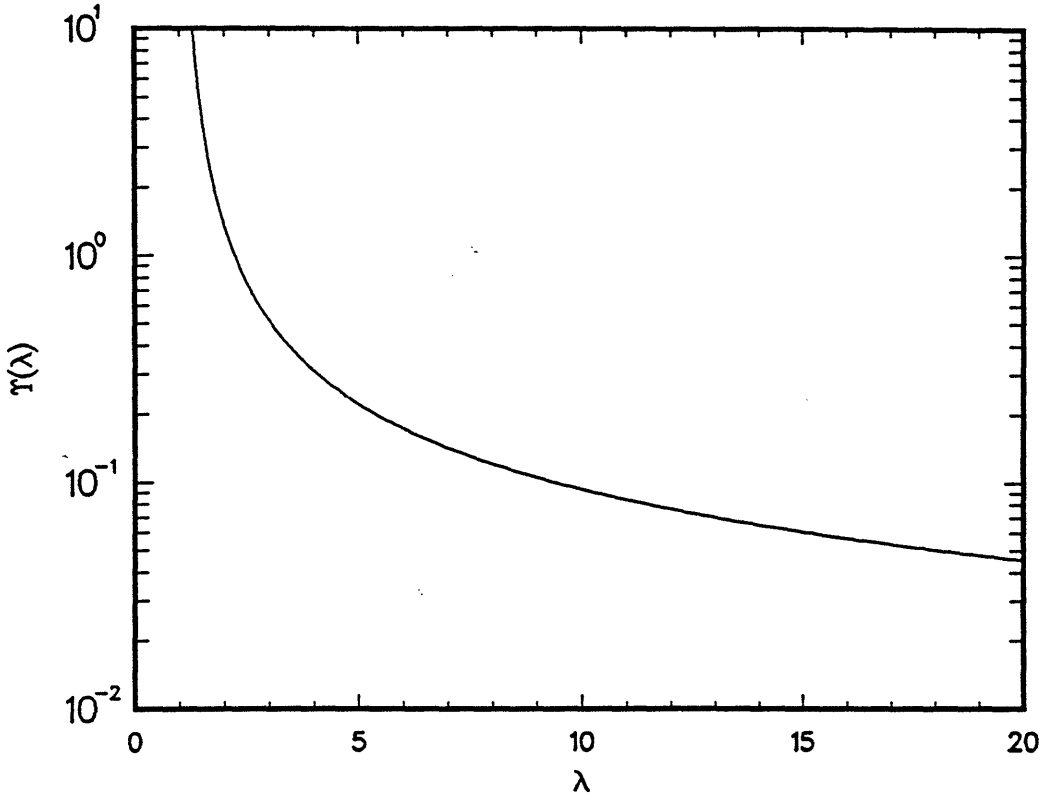

Fig. 7. Normalized orientation Cramer-Rao bound.

Index Terms

Reconstruction

Tomography

Projection

Object

Shape

Estimation

Performance

Parametric

Maximum Likelihood